ResearchGate

See discussions, stats, and author profiles for this publication at: https://www.researchgate.net/publication/230532562

Dual Phase-Controlled Synthesis of Uniform Lanthanide-Doped NaGdF4 Upconversion Nanocrystals Via an OA/Ionic Liquid Two-Phase System for In Vivo Dual-Modality Imaging

ARTICLE *in* ADVANCED FUNCTIONAL MATERIALS · DECEMBER 2011

Impact Factor: 11.81 · DOI: 10.1002/adfm.201101040

CITATIONS
97

READS
92

8 AUTHORS, INCLUDING:

Chunlei Zhang
Shanghai Jiao Tong University
52 PUBLICATIONS **1,131** CITATIONS
SEE PROFILE

Chenchen Bao
Shanghai Jiao Tong University
40 PUBLICATIONS **673** CITATIONS
SEE PROFILE

Guo Gao
Shanghai Jiao Tong University
50 PUBLICATIONS **971** CITATIONS
SEE PROFILE

Daxiang Cui
Shanghai Jiao Tong University
203 PUBLICATIONS **6,073** CITATIONS
SEE PROFILE

Available from: Chenchen Bao
Retrieved on: 16 January 2016

ADVANCED FUNCTIONAL MATERIALS
www.afm-journal.de

Dual Phase-Controlled Synthesis of Uniform Lanthanide-Doped $NaGdF_4$ Upconversion Nanocrystals Via an OA/Ionic Liquid Two-Phase System for In Vivo Dual-Modality Imaging

*Meng He, Peng Huang, Chunlei Zhang, Hengyao Hu, Chenchen Bao, Guo Gao, Rong He, and Daxiang Cui**

A novel OA/ionic liquid two-phase system combining the merits of thermal decomposition method, the IL-based strategy, and the two-phase approach is introduced to synthesize high-quality lanthanide-doped $NaGdF_4$ upconversion nanocrystals with different crystal-phases in OA-phase and IL-phase through a one-step controllable reaction. Oil-dispersible cubic-phase $NaGdF_4$:Yb, Er (Ho, Tm) nanocrystals with ultra-small size (~5 nm) and monodispersity are obtained in the OA phase of the two-phase system via an IL-based reaction. More importantly, water-soluble hexagonal-phase $NaGdF_4$:Yb, Er nanocrystals are obtained in the same system simply by adopting an extremely facile method to complete the dual phase-transition (crystal-phase transition and OA-phase to IL-phase transition) simultaneously. The synthesized lanthanide-doped $NaGdF_4$ upconversion nanocrystals are effective for dual-mode UCL imaging and CT imaging in vivo.

1. Introduction

Rare earth (RE) ions doped upconversion nanoparticles (UCNPs) have attracted much attention due to their attractive merits involving narrow emission peaks, large anti-stokes shifts, and low toxicity,[1] all of which lead to their potential applications in flat-panel displays, solid-state lasers, and especially in bio-imaging.[2] Among these materials, $NaGdF_4$ nanocrystals have been considered as an excellent luminescent host matrix for various optically active $Lanthanide^{3+}$ ions in both upconversion (UC) and downconversion (DC) luminescence.[3] Particularly, the unique magnetic resonance (MR) properties of Gd facilitate versatile applications as multiplexed luminescent nano-biolabels as well as MRI contrast agent. Very recently, Chen et al. reported the synthesis of $NaGdF_4$:Yb, Tm/$NaGdF_4$: Eu core–shell UCNPs and realized UC and DC luminescence simultaneously.[4] Li et al. studied in vivo imaging of the $NaGdF_4$:Yb, Er/Tm with dual-modality functions of near-infrared to near-infrared (NIR-NIR) upconversion luminescence and MRI.[5] Up to now, rare earth fluoride nanocrystals have been prepared by hydro(solvo) thermal reaction, thermal decomposition, and ionic liquids-based synthesis. Great efforts have been devoted to the synthesis of high-quality $NaREF_4$ nanocrystals through hydro (solvo) thermal reaction. However, it remains very difficult to synthesize hexagonal phase $NaREF_4$ nanocrystals (a structure exhibiting higher UC luminescent efficiency than cubic phase structure) while maintaining small size (<50 nm). Moreover, post-synthetic modification is usually needed for the products in a hydro(solvo) thermal system for further biological applications.[6] Up to date, thermal decomposition of trifluoroacetate precursors has been considered to be the most successful and commonly-used method to prepare hexagonal $NaREF_4$ UCNPs with small size (<50 nm) and high dispersity. Yet, it also exhibits some drawbacks involving rigorous experimental conditions, hazardous precursors and coordinating solvents and especially complicated surface modification of these hydrophobic products for biological compatibility.[7] Apart from using highly toxic trifluoroacetate precursors, Chen et. al. developed a modified and relatively facile thermal decomposition method by adopting simple $RE(oleate)_3$ as the precursors.[8]

Ionic liquids (ILs), due to their unique properties such as thermal and chemical stability, negligible vapor pressure, and wide electrochemical window,[9] have emerged as a promising medium for the synthesis of inorganic nanostructures such as metal oxides, metal alloys, metal fluorides and have been regarded as a "green" alternative to the conventional organic solvents.[10] Our group have recently successfully prepared monodisperse magnetite nanoparticles via an IL-assisted method.[11] Besides, previously reported attempts to synthesize hydrophilic

M. He,[†] Dr. P. Huang,[†] C. Zhang, H. Hu, C. Bao, G. Gao, Prof. R. He, Prof. D. Cui
Department of Bio-Nano Science and Engineering
National Key Laboratory of Micro/Nano Fabrication Technology
Key Laboratory of Thin Film and Microfabrication Technology of Department of Education
Institute of Micro-Nano Science and Technology
Shanghai Jiao Tong University
800 Dongchuan Road, Shanghai, 200240, China
E-mail: dxcui@sjtu.edu.cn
[†] M.H. and P.H. contributed equally to this work.

DOI: 10.1002/adfm.201101040

© 2011 WILEY-VCH Verlag GmbH & Co. KGaA, Weinheim

UCNPs in a one-pot IL-based reaction system, which was operated under mild conditions using innocuous reagents, provided an alternative to those conventional techniques. Kong et al.[12] and Chen et al.[13] have respectively obtained hexagonal and cubic $NaYF_4$:Yb, Er UCNPs featuring small size (<100 nm) and water-solubility in a one-step IL-based reaction. Unfortunately, the as-prepared products by IL-based method usually have poor shape-control, low dispersity and broad size distribution compared with those synthesized conventionally[14], and the study on the synthesis of RE fluoride in an IL-based system is still at its primary stage.

In short, the well-established synthetic strategies, including hydro(solvo) thermal synthesis thermal decomposition method, as well as the newly-developed IL-based synthesis still have their respective limitations in spite of the success in some respects. In order to combine the merits of the thermal decomposition method (size and morphology control, high-quality of products) and IL-based strategy (mild experimental conditions, user-friendly regents and direct water-solubility of products) while overcoming their respective defects, we adopt the notion of liquid-liquid two-phase approach by using $RE(oleate)_3$ as the precursors (the advantage of thermal decomposition method) and ILs as fluorine source (the advantage of IL-based stratagy). The two-phase strategy, with its intrinsic advantages, have been proved to be successful in the synthesis of high-quality nanoparticles.[15] Moreover, our group have recently reported a facile and controllable strategy to synthesize metallic nanocrystals in a liquid-liquid two-phase system.[16]

Herein, we devised a novel reaction system combining the advantages of thermal decomposition method, the IL-based strategy and the liquid-liquid two-phase approach. We introduced an oleic acid (OA)/1–butyl-3-methylimidazolium tetrafluoroborate ($BmimBF_4$) two-phase system to fabricate high-quality $NaGdF_4$:Yb, Er (Ho, Tm) nanocrystals with different crystal-phases in OA-phase and IL-phase through a one-step controllable reaction. We have, for the first time, obtained oil-dispersible cubic-phase $NaGdF_4$:Yb, Er (Ho, Tm) nanocrystals with ultra-small size (~5 nm) and monodispersity via an IL-based reaction. More importantly, we have obtained water-soluble hexagonal-phase $NaGdF_4$:Yb, Er nanocrystals in the same system simply by adopting an extremely facile method to complete the dual phase-transition (crystal-phase transition and OA-phase to IL-phase transition) simultaneously. Furthermore, in vivo dual-mode UCL imaging and CT imaging of lanthanide-doped $NaGdF_4$ upconversion nanocrystals were investigated.

2. Results and Discussion

In a typical procedure (see ESI†), $RE(oleate)_3$ complexes and sodium oleate were dissolved in oleic acid to form the top phase (OA-phase) of the two-phase system while $BmimBF_4$ formed the bottom phase (IL-phase). BF_4^- anions were partly decomposed to produce F^-, leading to the formation of $NaGdF_4$:Yb, Er nanocrystals. In this system, a certain volume of methanol played a pivotal role in controlling the dual phase-transition of $NaGdF_4$:Yb, Er nanocrystals. When no methanol was added, the reaction took place in OA-phase and the oleic acid capped UCNPs (OA-UCNPs) were formed. Finally, the oil-dispersible cubic-phase $NaGdF_4$:Yb, Er nanocrystals were obtained on the interface of the two-phase system. $BmimBF_4$ in IL-phase only acted as a fluorine source in this reaction. When 20 mL of methanol was added, water-soluble hexagonal-phase $NaGdF_4$:Yb, Er nanocrystals was formed in the IL-phase and the ionic liquid capped UCNPs (IL-UCNPs) were obtained. In this case, $BmimBF_4$ played many important roles such as template, fluorine source and capping agent.

The sizes and morphologies of the products were characterized by transmission electron microscopy (TEM). **Figure 1** shows the TEM images of oil-dispersible cubic-phase $NaGdF_4$: 20%Yb, 2%Er nanocrystals prepared without methanol. The average diameter of these ultrasmall nanoparticles in Figure 1a was 5.05 ± 0.83 nm, which was confirmed by a detailed analysis of the particle size of around 180 nanoparticles (see Figure S2a, Supporting Information (SI)). The nanoparticles appear spherical in shape and display high uniformity and monodispersity. The diffraction rings of the selected area electron diffraction (SAED) pattern (Figure 1c) could be ascribed to the (111), (200), (220), (311), (400), and (331) planes of cubic $NaGdF_4$ lattice. In addition, High-resolution TEM (HR-TEM) image (Figure 1d) reveals that these ultrasmall particles were highly crystalline and shows the lattice distance of 0.28 nm, corresponding to *d* spacing for the (200) lattice plane of the cubic $NaGdF_4$ structure.

Figure 2 shows the TEM images of water-soluble hexagonal-phase $NaGdF_4$: 20%Yb, 2%Er nanocrystals prepared with 20 mL of methanol. Similarly, these sphere-like particles are uniform in shape. However, these particles (Figure 2) have an average diameter of 21.04 ± 3.77 nm (see Figure S2b), larger than those oil-dispersible ones synthesized without methanol. The disparities in particle size and morphology can be attributable to the synthesis of hexagonal structure, which turned out

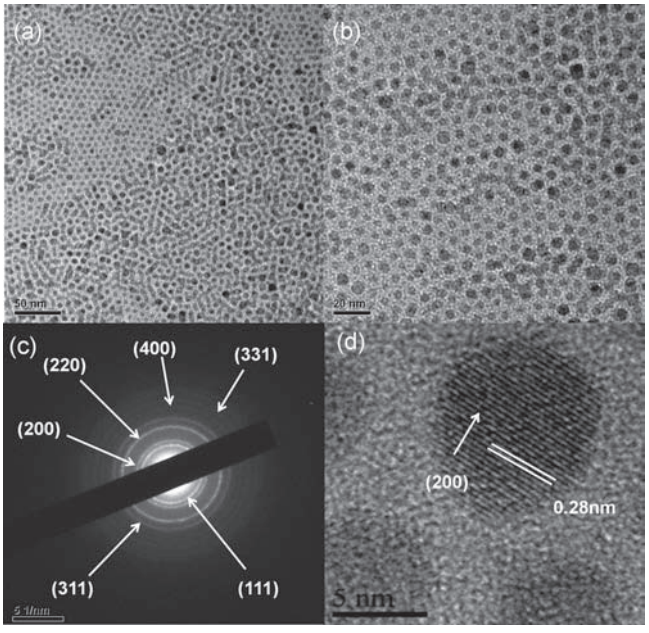

Figure 1. a,b) TEM images with different magnifications of oil-dispersible cubic-phase $NaGdF_4$: 20%Yb, 2%Er nanocrystals prepared without methanol. c) The SAED pattern. d) The corresponding HRTEM image.

© 2011 WILEY-VCH Verlag GmbH & Co. KGaA, Weinheim

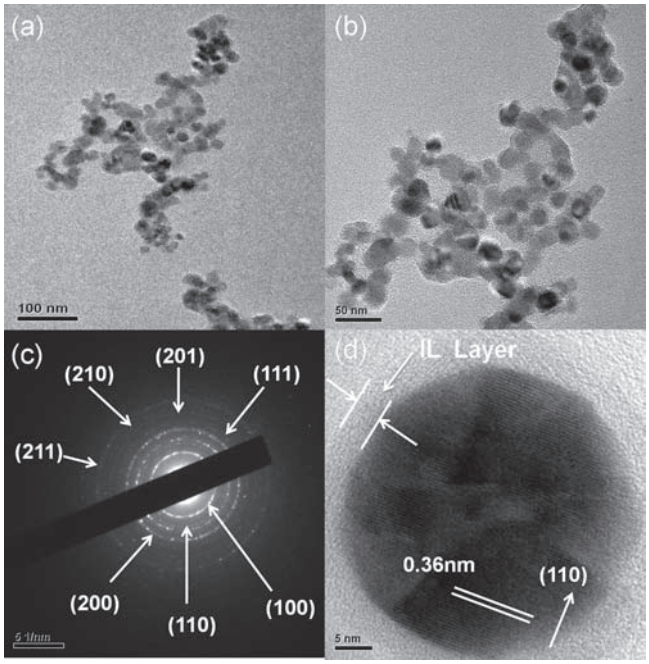

Figure 2. a,b) TEM images with different magnifications of water-soluble hexagonal phase $NaGdF_4$: 20%Yb, 2%Er nanocrystals prepared with 20mL of methanol. c) The SAED pattern. d) The corresponding HR-TEM image.

to exist in larger size than their cubic-phase counterparts[6d], as well as the change of reaction environment from OA-phase to IL-phase and to the difference in capping agents, both of which have a great impact on their nucleating and growing process. The SAED pattern in Figure 2c shows clear diffraction rings corresponding to the specific (100), (110), (200), (111), (201), (210), and (211) planes of hexagonal $NaGdF_4$ lattice, which indicates high crystallinity of the particles. In addition, HRTEM image (Figure 2d) shows the lattice distance of 0.36 nm, corresponding to *d* spacing for the (110) lattice plane of the hexagonal $NaGdF_4$ structure.

These results obviously show the crystal phase transition from cubic to hexagonal. Moreover, the change of capping agent can be demonstrated by the IL layer (marked by arrows in Figure 2d). The IL-layer absorbed on the surface of these particles made them disperse in water directly and suitable for facile surface modifications as well as further biological applications.

The crystal phase transition of the products was further characterized by X-ray diffraction (XRD) data in **Figure 3**. When no methanol was added (Figure 3a), the XRD pattern of $NaGdF_4$:20%Yb, 2%Er nanoparticles agrees well with the single-phase cubic $NaGdF_4$ crystals (JCPDS: 27-0697). When the volume of methanol increased to 2 mL (Figure 3b) and 10 mL (Figure 3c), their XRD patterns can be indexed as a mixture of cubic and hexagonal (JCPDS: 27-0699) phase of $NaGdF_4$ crystals. A gradual increase in peak intensities for hexagonal phase is observed as methanol increased. Eventually, the pure hexagonal $NaGdF_4$: 20%Yb, 2%Er nanocrystals were obtained when the volume of methanol reached 20 mL (Figure 3d). The peak positions and intensities accord with the single phase hexagonal $NaGdF_4$ crystals and no peaks of other phases or impurities are detected.

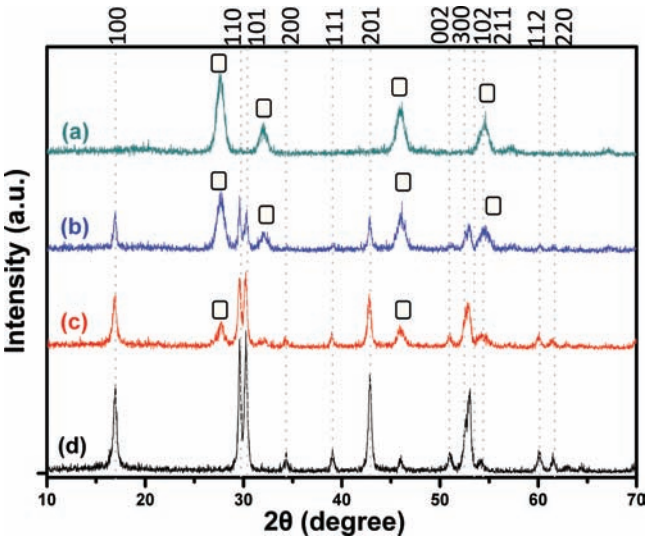

Figure 3. XRD patterns of $NaGdF_4$: 20%Yb, 2%Er nanocrystals when different ratios of methanol:IL (mL:mL) were added. a) 0:10; b) 2:23; c) 10:15; d) 20:5. Diffraction peaks of cubic $NaGdF_4$ are marked with square boxes. Different crystal planes of hexagonal $NaGdF_4$ lattice are marked with dotted lines.

As is shown in **Figure 4**, synthetic strategy 1 (A→B), marked by yellow arrow, shows the formation of cubic-phase oil-dispersible $NaGdF_4$:20%Yb, 2%Er nanocrystals prepared without methanol. Synthetic strategy 2 (A→C→D), marked by blue arrow, shows the formation of hexagonal-phase water-soluble $NaGdF_4$:20%Yb, 2%Er nanocrystals when methanol was added. Photographs of real products clearly show their final distribution (see Fig. S3, ESI). In the OA/IL two-phase system, RE $(oleate)_3$ complexes and sodium oleate were dissolved in oleic acid as precursors. $BmimBF_4$ in IL-phase partly decomposed under high temperature and produced F^-, leading to the formation of $NaREF_4$ nanocrystals.[17] When no methanol was added, the OA-phase and IL-phase were immiscible to each other even under high pressure and temperature. The reaction only took place on the interface area of the two-phase system. Due to the strong chelating capacity of oleic acid with RE^{3+} ions, the surface of the nanocrystals was covered by a layer of oleic acid, which prevented the particles from agglomerating and rendered them hydrophobic. Thus, we prepared oil-dispersible products in OA-phase. In this case, $BmimBF_4$ only acted as a fluorine source. When a certain volume of methanol was added, the methonal was soluble in both oleic acid and $BmimBF_4$ and therefore provided a "passageway" for RE^{3+} ions to transfer from OA-phase to IL-phase. Then RE^{3+} ions were surrounded by BF_4^- anions and $Bmim^+$ cations layer-by-layer due to coulombic or coordination interactions. When heated continuously, BF_4^- anions were degraded, resulting in the formation of $NaREF_4$ nanocrystals. Since this reaction was carried out in IL-phase, $BmimBF_4$ not only functioned as a fluorine source, but also as a template and capping/coordinating agent. The nucleating and growing process of the particles were shaped by the IL layer coordinated and absorbed on the surface, which ultimately decided their sizes and morphologies. Moreover, owning to the hydrophilic properties of

© 2011 WILEY-VCH Verlag GmbH & Co. KGaA, Weinheim

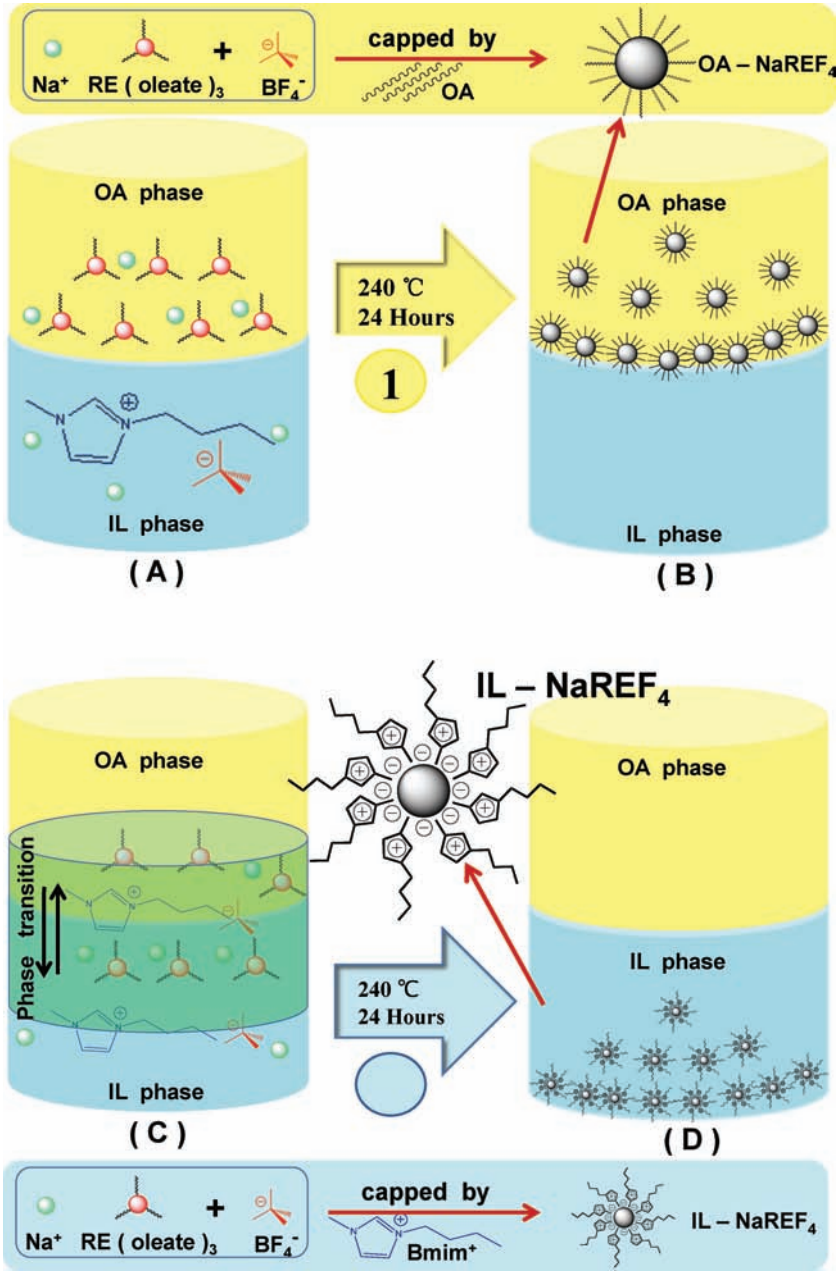

Figure 4. Schematic diagram showing the mechanism for the formation $NaGdF_4$ nanocrystals.

$BmimBF_4$ layer, these particles can be directly dispersed in water, which make them feasible for biological applications. The surface capping agents of products in OA-phase and IL-phase were further characterized by FTIR (see Figure S1).

In the case of crystal-phase transition from cubic to hexagonal, it can be reasonably speculated that the crystal-phase transition can be ascribed to the elevated concentration of F^- ions and the change in reaction environment of RE^{3+} ions. In a pure OA/IL two-phase system, the formation of $NaGdF_4$:Yb, Er nanocrystals only occurred in the interfacial area of the two-phase system due to the low inter-solubility of OA and $BmimBF_4$. It is rational to believe that the majority of RE^{3+} precursors were coordinated by oleic acid due to the strong coordinating capacity of OA. The interactions between BF_4^- ions and RE^{3+} precursors were quite limited and the effective concentration of F^- ions released from the cleavage of B-F bond in the formation of $NaGdF_4$ was quite low. So the synthesis of cubic phase products was favored. However, in a methanol-induced OA/IL two-phase system, the introduction of methanol successfully transferred all RE^{3+} precursors into IL phase and RE^{3+} ions were surrounded by $Bmim^+$ and BF_4^- ions through coordination and coulombic interactions. Therefore, the interactions between BF_4^- ions and RE^{3+} precursors were enhanced and effective concentration of F^- ions was elevated, which could effectively reduce the energy barrier from cubic-phase to hexagonal-phase.[18] On the other hand, the selective absorption of $Bmim^+$ and BF_4^- ions on the surface of the particles would facilitate their anisotropic growth in the IL phase and thus favored the fabrication of hexagonal phase structure.

It should be noted that the one-step synthesis of water-soluble products facilitate their further modification (including Stöber-based silica coating and layer-by-layer assembly of PSS and PAH) under mild conditions to enhance stability and bio-compatibility. The corresponding TEM images (Figure S4,S5, SI) and FT-IR spectra (Figure S6) are shown in supporting information.

The upconversion luminescence (UCL) spectra of Er^{3+}, Ho^{3+}, Tm^{3+} doped nanocrystals was is shown in **Figure 5**. The hexagonal (β) phase water-soluble products prepared with 20 mL methanol presented much higher luminescence intensities than those cubic (α) phase oil-dispersible ones synthesized without methanol. The main possible reason could be that the IL-UCNPs have a relatively larger size and smaller ratio surface, and thus less surface defects which are usually fluorescence quenchers.[19] On the other hand, a crystal phase change from cubic to hexagonal $NaREF_4$ offers at least an order of magnitude promotion of UC efficiency relative to its cubic commterparts.[20] As is shown in Figure 5a There are three emission peaks at around 520, 538 and 652 nm for $NaGdF_4$:20%Yb, 2%Er, corresponding to the $^2H_{11/2}$–$^4I_{15/2}$, $^4S_{3/2}$–$^4I_{15/2}$ and $^4F_{9/2}$–$^4I_{15/2}$ transitions of Er^{3+} respectively. In Figure 5b, the $NaGdF_4$:20%Yb, 2%Ho samples exhibit four distinct Ho^{3+} emission bands. The blue emissions at around 484 nm is originated from $^5F_3$–$^5I_8$ transition; the intense green emission at around 539 nm accounts for the $^5F_4$, $^5S_2$–$^5I_8$ transition; the weaker red and near-infrared (NIR) luminescence was ascribed to the $^5F_5$–$^5I_8$, and $^5F_4$, $^5S_2$–$^5I_7$ transitions of Ho^{3+} respectively. In the case of Tm^{3+} doped products(Figure 5c, d), five weak emission bands at around 445, 474, 538, 652 and

© 2011 WILEY-VCH Verlag GmbH & Co. KGaA, Weinheim

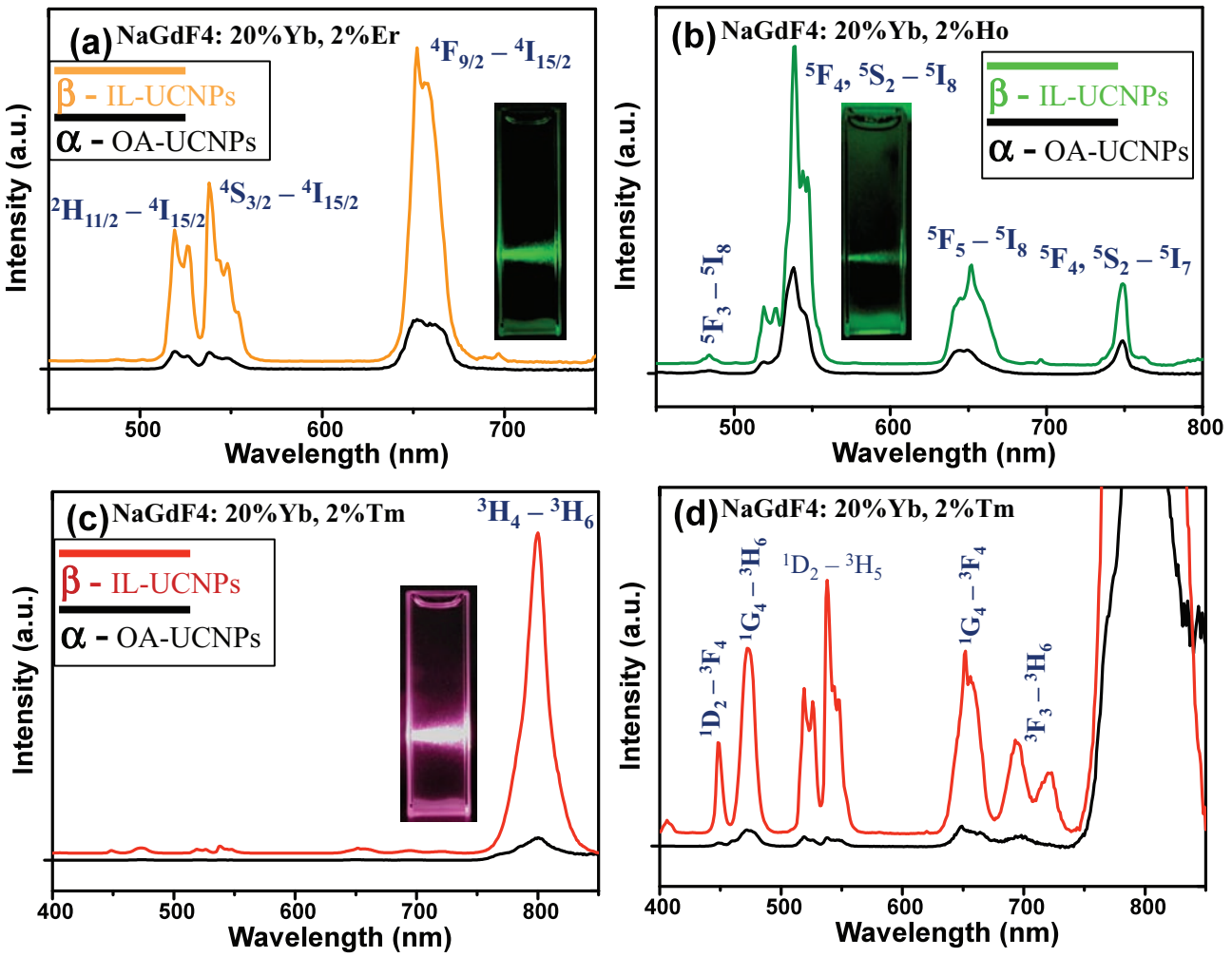

Figure 5. Upconversion luminescence spectra of a) $NaGdF_4$:20%Yb, 2%Er. b) $NaGdF_4$:20%Yb, 2%Ho. c) $NaGdF_4$:20%Yb, 2%Tm. d) the amplified UC spectrum of (c). Inset: The UC luminescent photographs of water-soluble β- $NaGdF_4$ UCNPs dispersed in water under 980 nm excitation.

693 nm was caused by $^1D_2$–$^3F_4$, $^1G_4$–$^3H_6$, $^1D_2$–$^3H_5$, $^1G_4$–$^3F_4$, and $^3F_3$–$^3H_6$ transitions of Tm^{3+} respectively. It is striking that the predominant NIR emission band peaked at around 800 nm, which is assigned to the $^3H_4$–$^3H_6$ transition, is much stronger than all other emission bands, indicating that radiative deactivation of the upconverted energy predominantly occurs through NIR luminescence, which is favorable for bioimaging.[21]

To demonstrate the feasibility of lanthanide-doped $NaGdF_4$ upconversion nanocrystals for in vivo dual-modality imaging, the water-soluble hexagonal-phase $NaGdF_4$:20%Yb, 2%Er was selected as a contrast reagent. **Figure 6** presents the in vivo whole-body images of nude mice without and with $NaGdF_4$:Yb, Er (100 µL 1 mg mL^{-1} per animal). The mice were imaged using a modified IVIS Lumina XR in which excitation was provided by the CW infrared laser at 980 nm. As is shown in Figure 6a, a clearly distinguished UCL signal was observed at the corresponding subcutaneous injection site, whereas no significant luminescence signal was observed in the control mice. Meanwhile, the subcutaneous injection site displayed an enhancer positive-contrast than other soft tissues (Figure 6b), which is attributed to that $NaGdF_4$:20%Yb, 2%Er induces a strong X-ray attenuation. The X-ray attenuation coefficient is determined by the atomic number and electron density, the higher the atomic number and electron density, the higher the attenuation

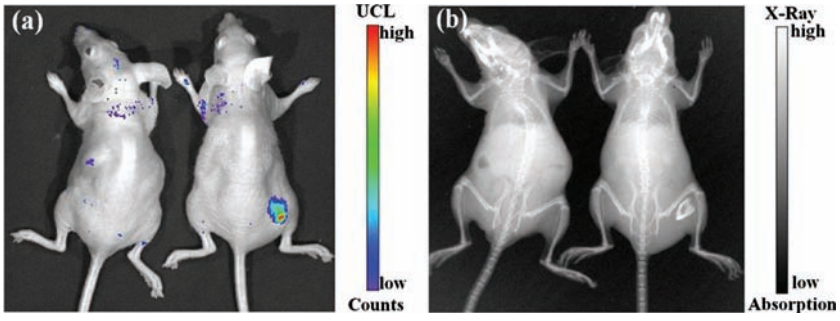

Figure 6. In vivo upconversion luminescence imaging (a) and X-ray imaging (b) of mice after subcutaneous injection (left) without and (right) with $NaGdF_4$: Yb, Er.

© 2011 WILEY-VCH Verlag GmbH & Co. KGaA, Weinheim

coefficient. The atomic number and electron density of Gd (64 and 7.895 g cm^{-3}, respectively) are much higher than those of the currently used iodine (53 and 4.9 g cm^{-3}).[22] The results indicated that the synthesized lanthanide-doped $NaGdF_4$ upconversion nanocrystals are effective for dual-mode UCL imaging and X-ray imaging in vivo.

Based on the absorption of X-ray, computed tomography (CT) can provide complementary anatomical information. Currently, CT contrast agents are typically low molecular weight and rapidly cleared by body in clinic.[22] Nanoparticle agents exhibited superior prolonged presence in the blood pool, which may make them suitable agents for vascular CT.[23] Therefore, we investigate the feasibility of lanthanide-doped $NaGdF_4$ upconversion nanocrystals for in vitro and in vivo CT imaging. **Figure 7**a displays the CT images in the range of 0.5–10 mg mL^{-1} of lanthanide-doped $NaGdF_4$ upconversion nanocrystals. As the mass concentration of lanthanide-doped $NaGdF_4$ upconversion nanocrystals increased, the CT signal intensity continuously increased resulting in brighter images. To further investigate the CT contrast effect, the attenuation values (HU) of lanthanide-doped $NaGdF_4$ upconversion nanocrystals at different concentrations were measured by a clinical CT (SIEMENS Spirit CT 31159, German). As shown in Figure 7b, HU as a function of the lanthanide-doped $NaGdF_4$ upconversion nanocrystals concentration display a well-correlated linear relationship ($R^2 = 0.9999$), described by the following typical equation: Y = 14.37-5.77X.

For in vivo CT imaging, the lanthanide-doped $NaGdF_4$ upconversion nanocrystals were injected into mice. The mice were imaged using the same CT as in vitro test. **Figure 8** presents the in vivo whole-body image of nude mice with lanthanide-doped $NaGdF_4$ upconversion nanocrystals (100 μL of 10 mg mL^{-1} per site). The corresponding injection site of mice displayed a clearly distinguished CT signal. Meanwhile, HU values of injection site is more than the values of other tissue (such as bone, muscle), indicating that the synthesized nanocrystals is effective for CT imaging in vivo. To the best of knowledge, it should be the first to be reported. Compared with traditional CT images, the as-prepared lanthanide-doped $NaGdF_4$ upconversion nanocrystals exhibit distinct advantages, however, so far it is not clarified well to compare with analogous ones using other Ln^{3+}-based NPs, which is under our further investigation. Keeping in mind that Gd^{3+} is a paramagnetic relaxation agent used in MRI, the multi-model in vivo imaging combining optical, CT and MR imaging is underway.

3. Conclusions

In summary, we have successfully synthesized high quality RE^{3+} doped $NaGdF_4$ nanocrystals with different properties in a newly-developed facile OA/IL two-phase system. Ultrasmall oil-dispersible cubic-phase OA-capped products with high uniformity and monodispersity were prepared in OA-phase. While water-soluble hexagonal-phase IL-capped products with uniform shape and size were synthesized in IL-phase. A certain volume of methanol has played a role of paramount importance in controlling the simultaneous dual phase-transition. In addition, we have demonstrated that the hydrophilic coatings and strong UCL of these IL-UCNPs were suited for UCL imaging and CT imaging in vivo. The multi-functional imaging system combining different modality such as optical, CT and

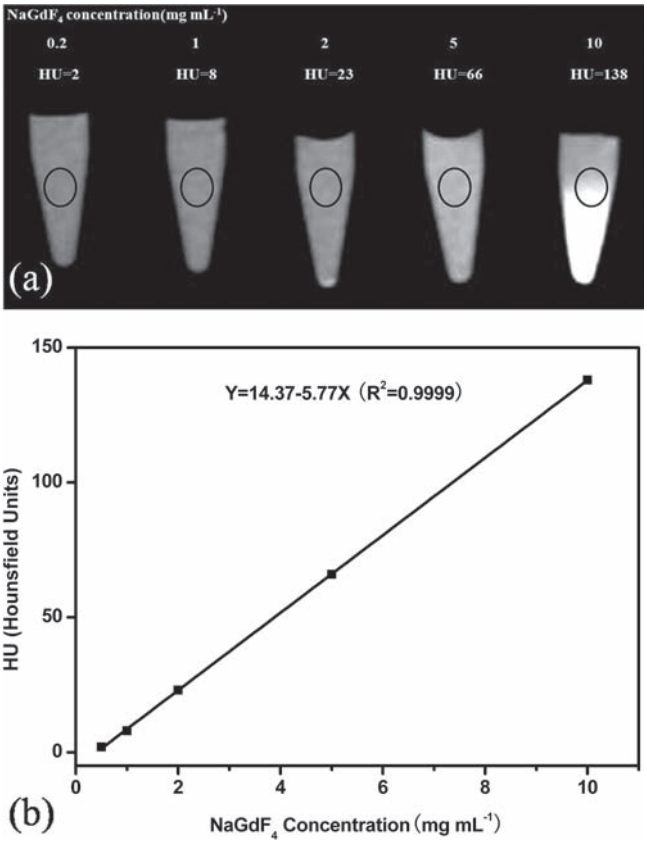

Figure 7. a) In vitro CT images of lanthanide-doped $NaGdF_4$ upconversion nanocrystals suspended in PBS. The concentration (mg mL^{-1}) in each sample is provided at the top of the respective images. b) CT attenuation (HU) of lanthanide-doped $NaGdF_4$ upconversion nanocrystals at various concentrations.

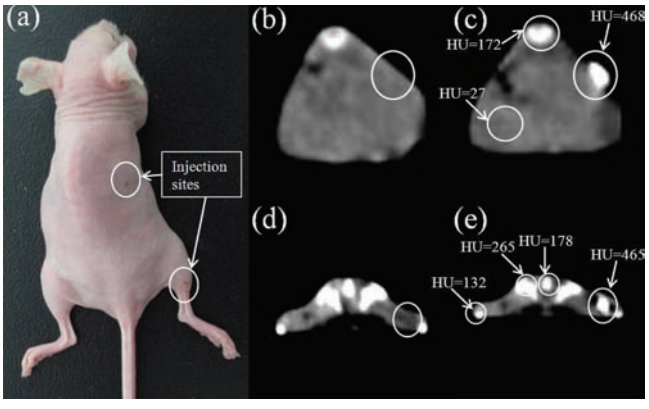

Figure 8. In vivo CT images of of mice after subcutaneous injection with lanthanide-doped $NaGdF_4$ upconversion nanocrystals suspended in PBS. a) The photograph of the injected mouse; b,c) the transverse image of the back, the HU value of the injection site is 468; d,e) the transverse image of the buttock, the HU value of the injection site is 465.

© 2011 WILEY-VCH Verlag GmbH & Co. KGaA, Weinheim

MR imaging could bring novel opportunities to the next generation of probes for the detection and imaging of biological targets in vivo.

4. Experimental Section

Materials: All the chemicals were of analytical grade and were used without further purification. Deionized water was used throughout. Rare earth oxides Gd_2O_3(99.99%), Yb_2O_3(99.99%), Er_2O_3(99.99%), Ho_2O_3(99.99%), and Tm_2O_3(99.99%) were purchased from Aladdin Chemistry Co. Ltd. Sodium oleate, oleic acid(OA), methanol were obtained from Sinopharm Chemical Reagent Co. 1–butyl-3-methylimidazolium tetrafluoroborate(BmimBF$_4$) was purchased from Henan Lihua Pharmaceutical Co. Ltd.

Synthesis of Rare Earth Oleate Complexes: RE (oleate)$_3$ complexes were prepared by previously reported methods.[24,25] One mmol of RE (oleate)$_3$[Gd: Yb: Er(Ho, Tm)] = [78: 20: 2] and a stoichiometric amount of sodium oleate was dissolved in 7 mL of oleic acid at elevated temperature under nitrogen atmosphere with vigorous magnetic stirring to form a homogeneous solution.

Synthesis of Oil-Dispersible Cubic-Phase NaGdF$_4$: Yb, Er (Ho, Tm) Nanocrystals in OA-phase: The as-prepared OA-phase containing Na^+ and RE (oleate)$_3$ was transferred into a 50-mL Teflon-lined autoclave which contained 10 mL of BmimBF$_4$. The two phase system was treated at 240 °C for 24 hours. After cooling to room temperature naturally, the precipitates were found on the interface of the two phase system. Then they were washed by cyclohexane and ethanol several times under ultrasonic conditions and were collected through centrifugation at 9500 rpm. Finally, the products are dried at 70 °C under vacuum for 12 hours.

Synthesis of Water-Soluble Hexagonal-Phase NaGdF$_4$: Yb, Er (Ho, Tm) Nanocrystals in IL-Phase: The synthetic procedure was the same as that used to prepare the oil-dispersible products except that 20 mL of methanol was added to the two-phase system and that the volume of BmimBF$_4$ was reduced to 5 mL. In contrast, the all the precipitates were found in the ionic-liquid phase.

Characterization: The sizes and morphologies of the products were characterized by transmission electron microscopy (TEM) using a JEM 2010 microscopy (JEOL, Japan) and High-resolution TEM (HRTEM) on JEM 2100F microscopy (JEOL, Japan) with an acceleration voltage of 200 kV. Powder X-ray diffraction (XRD) analysis was performed on a Dmax-r C X-ray diffractometer (Rigaku, Japan) with Cu K*a* radiation at 1.540 A° at a scanning rate of 6°/min in the 2θ range from 10°–70°. Fourier transform infrared (FT-IR) spectra were measured by EQUINOX 55 spectrometer (Bruker, Germany) from samples on KBr pellets. Upconversion fluorescence spectra were recorded on Fluorolog-3 spectrofluorometer (Jobin Yvon, France) at room temperature.

Animal Experiments and In Vivo Dual-Modality Imaging: Male nude mice weighing 20~22 g were purchased from Shanghai SLAC Laboratory Animal Co. Ltd (Shanghai, China). All animal procedures were in agreement with institutional animal use and care regulations. In vivo dual-modality UCL imaging and X-ray imaging were performed with a modified IVIS Lumina XR (Xenogen Corporation-Caliper, Alameda, CA, USA) using an external 0~5 W adjustable CW infrared laser (980 nm, Shanghai Connet Fiber Optics Co., China) as the excited source. Nude mice were randomized into two groups of three animals per group including control group and subcutaneous injection group. After mice were anesthetized (with 100 μL 10% chloral hydrate), for subcutaneous injection group, the water-soluble hexagonal-phase NaGdF$_4$: Yb, Er aqueous solution (100 μL 1 mg mL^{-1}) in 0.9% NaCl saline solution was subcutaneously injected into the right rear flank area. Then the optical/X-ray whole-body images of mice were recorded on IVIS Lumina XR instrument. For in vivo CT imaging, the NaGdF$_4$: Yb, Er aqueous solution (100 μL 10 mg mL^{-1} per site) in PBS was subcutaneously injected into the back of mice, and was intramuscularly injected into the right hind leg of mice, respectively. All CT scans were performed using a clinical CT (SIEMENS Spirit CT 31159, German).

Supporting information

Supporting Information is available from the Wiley Online Library or from the author.

Acknowledgements

This work is supported by National 863 Hi-tech Project of China (No. 2007AA022004), National Key Basic Research Program (973 Project) (No. 2010CB933901 and 2011CB933100), Important National Science & Technology Specific Projects (2009ZX10004-311), National Natural Scientific Fund (No. 20803040), New Century Excellent Talent of Ministry of Education of China (NCET-08-0350), Shanghai Science and Technology Fund (No. 10XD1406100), and Shanghai Jiao Tong University Innovation Fund for Postgraduates.

Received: May 10, 2011
Published online: September 22, 2011

[1] a) F. Wang, X. G. Liu, *Chem. Soc. Rev.* **2009**, *38*, 976; b) F. Wang, D. Banerjee, Y. S. Liu, X. Y. Chen, X. G. Liu, *Analyst* **2010**, *135*, 1839; c) H. S. Mader, P. Kele, S. M. Saleh, O. S. Wolfbeis, *Curr. Opin. Chem. Biol.* **2010**, *14*, 582; d) L. D. Carlos, R. A. S. Ferreira, V. De Zea Bermudez, S. J. L. Ribeiro, *Adv. Mater.* **2009**, *21*, 509; e) J. C. G. Bünzli, *Chem. Rev.* **2010**, *110*, 2729.

[2] a) C. Wang, L. Cheng, Z. Liu, *Biomaterials* **2011**, *32*, 1110; b) L. Cheng, K. Yang, S. Zhang, M. W. Shao, S. T. Lee, Z. Liu, *Nano Res.* **2010**, *3*, 722; c) C. X. Liu. *Nano Biomed Eng.* **2009**, *1*, 1; d) D. X. Cui, Y. D. Han, Z. M. Li, H. Song, K. Wang, R. He, B. Liu, H. L. Liu, C. C. Bao, P. Huang, J. Ruan, F. Gao, H. Yang, H. S. Cho, Q. S. Ren, D. L. Shi. *Nano Biomed Eng.* **2009**, *1*, 61; e) P. Huang, Z. Li, J. Lin, D. P. Yang, G. Gao, C. Xu, L. Bao, C. L. Zhang, K. Wang, H. Song, H. Y. Hu, D. X. Cui, *Biomaterials* **2011**, *32*, 3447; f) Z. Li, P. Huang, X. Zhang, J. Lin, S. Yang, B. Liu, F. Gao, P. Xi, Q. Ren, D. X. Cui, *Mol. Pharm.* **2009**, *7*, 94; g) P. Huang, C. Xu, J. Lin, C. Wang, X. Wang, C. Zhang, X. Zhou, S. Guo, D. X.Cui, *Theranostics*, **2011**, *1*, 240.

[3] a) F. Wang, X. Fan, M. Wang, Y. Zhang, *Nanotechnology* **2007**, *18*, 025701; b) C. H. Liu, H. Wang, X. R. Zhang, D. P. Chen, *J. Mater. Chem.* **2009**, *19*, 489; c) J. C. Boyer, J. Gagnon, L. A. Cuccia, J. A. Capobianco, *Chem. Mater.* **2007**, *19*, 3358; d) P. Ptacek, H. Schäfer, K. Kömpe, M. Haase, *Adv. Funct. Mater.* **2007**, *17*, 3843; e)Y. I. Park, J. H. Kim, K. T. Lee, K. S. Jeon, H. B. Na, J. H. Yu, H. M. Kim, N. Lee, S. H. Choi, S. I. Baik, H. Kim, S. P. Park, B. J. Park, Y. W. Kim, S. H. Lee, S. Y. Yoon, I. C. Song, W. K. Moon, Y. D. Suh, T. Hyeon, *Adv. Mater.* **2009**, *21*, 4467.

[4] Y. S. Liu, D. T. Tu, H. M. Zhu, R. F. Li, W. Q. Luo, X.Y. Chen, *Adv. Mater.* **2010**, *22*, 3266.

[5] J. Zhou, Y. Sun, X. X. Du, L. Q. Xiong, H. Hu, F. Y. Li, *Biomaterials* **2010**, *31*, 3287.

[6] a) Z. G. Chen, H. L. Chen, H. Hu, M. X. Yu, F. Y. Li, Q. Zhang, Z. G. Zhou, T. Yi, C. H. Huang, *J. Am. Chem. Soc.* **2008**, *130*, 3023; b) Z. Q. Li, Y. Zhang, *Angew. Chem., Int. Ed.* **2006**, *45*, 7732; c) X. Wang, Y. D. Li, *Nature* **2005**, *437*, 121; d) F. Wang, Y. Han, C. S. Lim, Y. H. Lu, J. Wang, J. Xu, H. Y. Chen, C. Zhang, M. H. Hong, X. G. Liu, *Nature* **2010**, *463*, 1061.

[7] a) H. X. Mai, Y. W. Zhang, R. Si, Z. G. Yan, L. S. Sun, L. P. You, C. H. Yan, *J. Am. Chem. Soc.* **2006**, *128*, 6426; b) J. C. Boyer, F. Vetrone, L. A. Cuccia, J. A. Capobianco, *J. Am. Chem. Soc.* **2006**, *128*, 7444; c) G. S. Yi, G. M. Chow, *Chem. Mater.* **2007**, *19*, 341.

[8] C. H. Liu, H. Wang, X. Li, D. P. Chen, *J. Mater. Chem.* **2009**, *19*, 3546.

[9] a) P. Hapiot, C. Lagrost, *Chem. Rev.* **2008**, *108*, 2238; b) K. Ding, Z. Miao, Z. Liu, Z. Zhang, B. Han, G. An, S. Miao, Y. Xie, *J. Am. Chem. Soc.* **2007**, *129*, 6362; c) H. J. Ryu, L. Sanchez, H. A. Keul, A. Raj, M. R. Bockstaller, *Angew. Chem. Int. Ed.* **2008**, *47*, 7639.

© 2011 WILEY-VCH Verlag GmbH & Co. KGaA, Weinheim

[10] a) M. Antonietti, D. Kuang, B. Smarsly, Y. Zhou, *Angew. Chem. Int. Ed.* **2004**, *43*, 4988; b) C. Burda, X. B. Chen, R. Narayanan, M. A. EI-Sayed, *Chem. Rev.* **2005**, *105*, 1025; c) K. Biswas, C. N. R. Rao, *Chem.–Eur. J.* **2007**, *13*, 6123; d) D. S. Jacob, L. Bitton, J. Grinblat, I. Felner, Y. Koltypin, A. Gedanken, *Chem. Mater.* **2006**, *18*, 3162; e) Y. J. Zhu, W. W. Wang, R. J. Qi, X. L. Hu, *Angew. Chem. Int. Ed.* **2004**, *43*, 1410; f) Y. Jiang, Y. J. Zhu, G. F. Cheng, *Crystal Growth & Design* **2006**, *6*, 2174; g) W. W. Wang, Y. J. Zhu, *Crystal Growth & Design* **2005**, *5*, 505; h) C. Lorbeer, J. Cybinska, A. V. Mudring, *Chem. Commun.* **2010**, *63*, 571; i) N. V. Prondzinski, J. Cybinska, A. V. Mudring, *Chem. Commun.* **2010**, *46*, 4393.

[11] H. Y. Hu, H. Yang, P. Huang, D. X. Cui, Y. Q. Peng, J. C. Zhang, F. Y. Lu, J. Lian, D. L. Shi, *Chem. Commun.* **2010**, *46*, 3866.

[12] X. M. Liu, J. W. Zhao, Y. J. Sun, K. Song, Y. Yu, C. Du, X. G. Kong, H. Zhang, *Chem. Commun.* **2009**, *43*, 6628.

[13] C. Zhang, J. Chen, *Chem. Commun.* **2010**, *46*, 592.

[14] C. X. Li, J. Lin, *J. Mater. Chem.* **2010**, *20*, 6831.

[15] a) D. Pan, Q. Wang, L. An, *J. Mater. Chem.* **2009**, *19*, 1063; b) J. Yang, J. Ying, *Nat. Mater.* **2009**, *8*, 683.

[16] P. Huang, J. Lin, Z. M. Li, H. Y. Hu, K. Wang, G. Gao, R. He, D. X. Cui, *Chem. Commun.* **2010**, *46*, 4800.

[17] a) C. N. R. Rao, S. R. C. Viekchand, K. Biswas, A. Govindaraj, *Dalton Trans.* **2007**, 3728; b) C. Zhang, J. Chen, Y. Zhou, D. Li, *J. Phys. Chem. C*, **2008**, *112*, 10083.

[18] P. Ghosh, A. Patra, *J. Phys. Chem. C*, **2008**, *112*, 3223.

[19] F. Wang, J. Wang, X. G. Liu, *Angew. Chem. Int. Ed.* **2010**, *49*, 7456.

[20] S. Heer, K. Kompe, H. U. Güdel, M. Hasse, *Adv. Mater.* **2004**, *16*, 2102.

[21] G. Y. Chen, Y. G. Zhang, G. Somesfalean, Z. G. Zhang, *Appl. Phys. Lett.* **2006**, *89*, 163105; b) G. Y. Chen, T. Y. Ohulchanskyy, R. Kumar, H. Agren, P. N. Prasad, *Acs nano.* **2010**, *6*, 3163.

[22] R. Popovtzer, A. Agrawal, N. A. Kotov, A. Popovtzer, J. Balter, T. E. Carey, R. Kopelman, *Nano Lett.* **2008**, *8*, 4593.

[23] S. M. Janib, A. S. Moses, J.A. MacKay, *Adv Drug Deliv Rev.*,**2010**, *62*, 1052.

[24] Y. Wei, F. Q. Lu, X. R. Zhang, D. P. Chen, *Chem. Mater.* **2006**, *18*, 5733.

[25] J. Park, K. J. An, Y. S. Hwang, J. G. Park, H. J. Noh, J. Y. Kim, J. H. Park, N. M. Hwang, T. Hyeon, *Nat. Mater.* **2004**, *3*, 891.

© 2011 WILEY-VCH Verlag GmbH & Co. KGaA, Weinheim